THE JOURNAL OF PHYSICAL CHEMISTRY A

ARTICLE

pubs.acs.org/JPCA

Single-Shot Gradient-Assisted Photon Echo Electronic Spectroscopy

Elad Harel, Andrew F. Fidler, and Gregory S. Engel*

The James Franck Institute and Department of Chemistry, University of Chicago, Chicago, Illinois 60637, United States

ABSTRACT: Two-dimensional electronic spectroscopy (2D ES) maps the electronic structure of complex systems on a femtosecond time scale. While analogous to multidimensional NMR spectroscopy, 2D optical spectroscopy differs significantly in its implementation. Yet, 2D Fourier spectroscopies still require point-by-point sampling of the time delay between two pulses responsible for creating quantum coherence among states. Unlike NMR, achieving the requisite phase stability at optical frequencies between these pulse pairs remains experimentally challenging. Nonetheless, 2D optical spectroscopy has been successfully demonstrated by combining passive and active phase stabilization along with precise control of optical delays and long-term temperature stability, although the widespread adoption of 2D ES has been significantly hampered by these technical challenges. Here, we exploit an analogy to magnetic resonance imaging (MRI) to demonstrate a single-shot method capable of acquiring the entire 2D spectrum in a single laser shot using only conventional optics. Unlike point-by-point sampling protocols typically used to record 2D spectra, this method, which we call GRadient-Assisted Photon Echo (GRAPE) spectroscopy, largely eliminates phase errors while reducing the acquisition time by orders of magnitude. By incorporating a spatiotemporal encoding of the nonlinear polarization along the excitation frequency axis of the 2D spectrum, GRAPE spectroscopy achieves no loss in signal while simultaneously reducing overall noise. Here, we describe the principles of GRAPE spectroscopy and discuss associated experimental considerations.

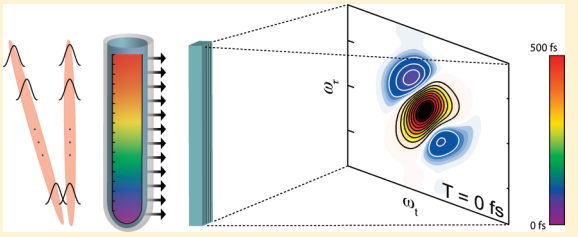

Ultrafast nonlinear spectroscopy can monitor vibrational and electronic dynamics in complex systems on a femtosecond time scale.[1−3] As the complexity of the system increases, one-dimensional techniques no longer provide unambiguous assignment of energy eigenstates and their associated relaxation dynamics because couplings can only be measured indirectly. The extension of these methods to two-dimensions with 2D photon echo spectroscopy[4−6] provides a direct probe of molecular structure, electronic coupling, energy transfer, and solute−solvent dynamics in the IR and visible regions of the electromagnetic spectrum. The potential of multidimensional spectroscopy in the optical regime was first recognized by Ernst during the development of 2D NMR.[7] Because of the need to record the signal as a function of two or more temporal dimensions of which only one is available for direct detection, multidimensional spectroscopy necessarily involves parametric sampling of one or more time delays. Unlike NMR where electronic gating permits near-arbitrary phase and temporal control, controlling propagating beams of light requires adjustments of optical path lengths to subwavelength accuracy. In the visible or UV, small errors in path length due to fluctuations in mirror positions and delay stages, index of refraction changes from eddies in the air, and temperature fluctuations in the environment all lead to phase errors that manifest themselves in the 2D spectrum as increased noise and broadened line widths. To date, successful implementation of two-dimensional optical spectroscopy has relied on either passive or active phase stabilization to limit these errors to provide a usable experimental window in which to carry out the data acquisition. In this manuscript, we demonstrate a new acquisition method, which we term GRadient-Assisted Photon Echo (GRAPE) spectroscopy that can eliminate the need for phase stabilization by acquiring the entire 2D spectrum in a single laser shot with higher signal-to-noise than is achievable with point-by-point acquisition protocols currently in use. In this report, we will outline the principles behind GRAPE spectroscopy as well as discuss its experimental implementation and challenges.

TWO-DIMENSIONAL PHOTON ECHO SPECTROSCOPY

The principles of 2D optical spectroscopy have been reported and discussed in detail elsewhere.[5,6,8−11] Briefly, 2D ES is a degenerate four-wave mixing spectroscopy that reveals the correlation between the absorption and emission frequencies of a material system. The 2D spectrum, generated by measuring the third-order nonlinear polarization in a unique phase matched direction, links the dipole oscillation frequency during an initial period, τ, with that of a final period, t, for each "population time" T. Peaks appearing on the diagonal provide a measure of the "memory" of the system in which an oscillating dipole at a given frequency is correlated to the same oscillator a time T later.

Special Issue: Graham R. Fleming Festschrift

Received: July 27, 2010
Revised: October 3, 2010
Published: November 23, 2010

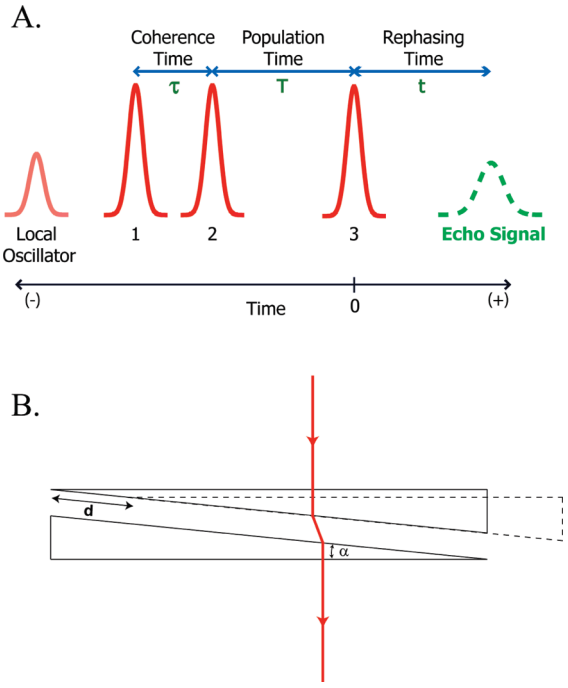

Figure 1. (A) 2D photon echo pulse sequence. Pulse 1 creates a single-quantum coherence between ground and excited states of the system, which evolves for a coherence time, τ. Pulse 2 stores the phase acquired during the coherence time as a population for a population time, T. Pulse 3 then returns the system to a single-quantum coherence where, for inhomogeneously broadened systems, a photon echo forms after a rephasing time $t \approx \tau$. The photon echo interferes with a weak local oscillator (LO) pulse at the spectrometer to retrieve phase and amplitude information during detection. (B) Glass wedge delay. Two antiparallel glass wedges are used to create subwavelength accuracy delays between pulses 1 and 2. Movement of one wedge along a wedge angle, α, by a distance d creates a delay of approximately $\alpha d/c$ for small angles without changing the direction of the propagating beam.

Cross-peaks provide information on electronic coupling between dipoles. Changes in the 2D spectrum as a function of the waiting time reveal the dynamics of energy transfer among chromophores as well as interactions of chromophores with their surroundings. In the case of the photon echo, inhomogeneous broadening along the direct t-domain is reduced to the homogeneous limit, making it particularly useful for systems with broad or featureless linear spectra.[12] 2D ES has successfully elucidated dynamics and microscopic interactions in semiconductor quantum wells,[13] carbon nanotubes,[14,15] photosynthetic light-harvesting complexes,[4,16] and other complex multichromophoric systems on an ultrafast time scale. For short population times, 2D optical spectroscopy is an analog of the 2D NMR COSY experiment, while for long population times it is conceptually similar to the 2D NMR NOESY experiment.[11,17,18]

In 2D photon echo experiments, a femtosecond laser pulse is split into four identical beams by using beam splitters or diffractive optics in the noncollinear geometry or by an acoustic optic modulator (AOM) in the collinear configuration. All four beams are focused onto $a < 100\ \mu$m diameter spot in the sample; the signal is then heterodyned and spectrally resolved using a spectrometer and CCD camera in the noncolinear geometry or fluorescence detected in the collinear geometry. The pulse sequence is shown in Figure 1A. The first pulse, $\mathbf{k}_1$, generates a one-quantum coherence in the sample that evolves for a specific amount of time, τ, before application of the second pulse, $\mathbf{k}_2$, that stores the phase as a population. The third pulse, $\mathbf{k}_3$, is then delayed by a population time, T, before the system is brought back to a single-quantum coherence, where detection by heterodyning with the fourth pulse, $\mathbf{k}_4$, occurs. The signal for each emitted frequency is then recorded as a function of the two delay times, τ and T.

The various experimental apparatuses differ primarily in the way the delays are generated. In the most common apparatus to date, the τ delay is created by accurate positioning of pairs of identical glass wedges in an antiparallel orientation mounted on linear translation stages;[8] each set of wedges essentially acts like a glass plate of varying thickness (Figure 1B). Delays can also be generated by use of pulse shaping technology such as spatial light modulation (SLM)[19] or acoustic optic modulation.[20] In each case, τ is systematically scanned for each population time to sample the optical frequency of the signal or, for rotating frame detection, the largest difference frequency of the oscillating dipoles in the sample. Because of the Fourier nature of this sampling, phase stability, either passive or active, is the single most important consideration for successful implementation of coherent multidimensional spectroscopy, particularly in the visible region of the spectrum.[8,21]

SPATIAL ENCODING

In the limit of zero pulse-front tilt (i.e., no angular dispersion or spatial chirp), the wavefront of a beam of light is perpendicular to its direction of propagation. For a well-collimated beam, the wavefront is approximately flat. In the absence of spatial chirp, when two noncollinear beams cross, their wavefronts are tilted with respect to one another, resulting in a time delay that is proportional to their position along the beam waist. This temporal gradient is dependent on the crossing angle, α, and is given by $(\tan \alpha)/c$. For example, the maximum time delay across a 5 mm beam waist for a crossing angle of 1° is 291 fs, within the range of single-quantum coherence lifetimes for many systems exhibiting electronic transitions in the visible region of the spectrum such as the laser dye examined here. If the time delay between pulses 2 and 3 remains constant, then each spatial location across the sample uniquely maps to a different four-wave mixing experiment, equivalent to parametric sampling of the τ delay for a fixed population time, T, as shown in Figure 2. After passage through a spectrometer, the resultant 2D image forms an instantaneous snapshot of a 2D photon echo spectrum for a fixed population time.

We limit our discussions in this report to apparatuses that do not include diffractive optics. Diffractive optics are not necessary for GRAPE, and diffractive beam splitters as currently used by many practioners of two-dimensional optical spectroscopy are problematic in a single-shot design because of angular dispersion. In point-by-point methods, the point of focus from which the four beams originate is imaged onto the sample so that angular dispersion does not present a problem. That is, all colors, even though they are diffracted in different directions by the grating, are then refocused onto the sample and hence arrive at the same moment in time. This same approach cannot be used with a line of focus since the GRAPE apparatus is a imaging spectrometer; the focusing in the horizontal caused by the cylindrical mirror is separate from the vertical tilts dictated by flat mirrors in the GRAPE mirror assembly, which define the temporal gradient. Use of diffractive optics would result in different temporal

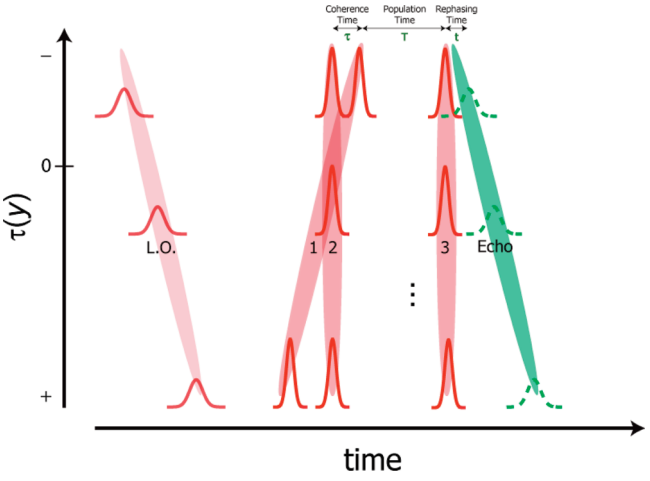

Figure 2. Spatially encoded 2D pulse sequence. Tilted wavefronts serve to define the pulse sequence along the *y*-axis of the sample. Wavefronts of beams 2 and 3 are parallel, which act to define a constant population time, *T*, across the sample. Wavefronts of beams 1 and 4 are tilted in opposite directions relative to beams 2 and 3, creating a spatially encoded temporal delay, $\tau(y)$. Each position along the *y*-axis of the sample uniquely maps to a single delay of the coherence time, τ, which in aggregate defines the entire 2D photon echo pulse sequence. The CCD camera then acts to bin a range of coherence times ($\Delta\tau \sim 0.5$ fs) for each pixel.

gradients for each spectral component of the pulse as well as chirp in the spatial axis. Fortunately, the use of diffractive optics is not needed in GRAPE because of the inherent phase stability of the system.

PHASE MATCHING

The conventional boxcar geometry (Figure 3A) used for phase matching in 2D ES in which all four pulses are focused to an isotropic beam waist creates a temporal gradient between all pairs of pulses. This effect, present in all noncollinear multiwave mixing experiments, causes a slight temporal smearing of the pulses due to the crossing angle and finite beam waist. For small fixed crossing angles, less than a few degrees, this smearing is roughly proportional to the beam waist. In point-by-point 2D ES, where the signal is integrated over the focal volume, the beam waist is kept small (<100 μm) to minimize this smearing to less than a few femtoseconds.[22] However, for a large beam waist (>5 mm) this smearing would be on the order of a few hundred femtoseconds, precluding the accurate acquisition of 2D spectra.

Now consider the phase-matched geometry shown in Figure 3B. Instead of focusing to a point, the beams now focus to a line perpendicular to the direction of propagation and the line connecting beams 2 and 3. At each position along the vertical axis of the focal plane, a small temporal smearing of the pulses exists due to the finite horizontal beam waist (<100 μm); however, the wavefronts of beams 2 and 3 are exactly parallel in the unfocused direction, resulting in the spatially encoded pulse sequence shown in Figure 2. The signal, emitted from the sample in the direction, $\mathbf{k}_s = -\mathbf{k}_1 + \mathbf{k}_2 + \mathbf{k}_3$, is now in the form of a line, rather than a point. Imaging this line onto a spectrometer input slit results in a two-dimensional map with the τ delay along the vertical direction (y) and wavelength along the horizontal direction (x). The image shares similarities with the trace formed by transient grating frequency-resolved optical gating (TG FROG) used for pulse characterization.[23] Unlike TG FROG, the signal is phase resolved by interference with a reference pulse. Fourier transformation of this two-dimensional signal along the τ direction yields the two-dimensional spectrum of the material system.

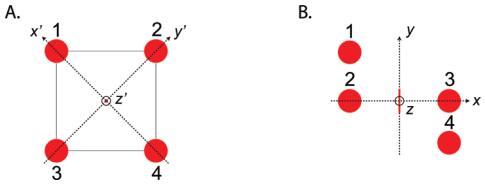

Figure 3. (A) Boxcar geometry. This phase-matched geometry provides passive phase stability for point-by-point acquisition methods. The rephasing signal is emitted in the direction, $\mathbf{k}_s = -\mathbf{k}_1 + \mathbf{k}_2 + \mathbf{k}_3$, which coincides with the local oscillator pulse labeled as beam 4 in the bottom right-hand side of the square. (B) Distorted box-car geometry for GRAPE. This phase-matched geometry provides passive phase stability for single-shot acquisition. The beams are focused in a direction parallel to the *y*-axis. This scheme allows beams 2 and 3 to maintain parallel wavefronts at the sample, while introducing a temporal gradient, $dt_{1,2(3)}/dy$ between beams 1 and 2 (3). Beam 4 (i.e., L.O.) coincides with the rephasing signal and has an opposite temporal gradient, $dt_{4,2(3)}/dy \approx -dt_{1,2(3)}/dy$, with respect to 2(3).

PREVIOUS SINGLE-SHOT OPTICAL TECHNIQUES

The idea to use space to encode time has been around for some time in optical spectroscopy. As early as 1971, echelon structures were used to subdivide the transverse profile of a beam into multiple pulses,[24] each delayed by a different amount depending on the glass composition and step size. More recently, Poulin et al used an echelon structure to monitor the irreversible photolysis of ions in organic crystals in real time using a single-shot pump−probe setup.[25] The same group used crossed femtosecond pulses to record single-shot pump-probe signals across multiple time points.[26] Undoubtedly, the most prevalent use of spatial encoding by crossed beams is for pulse characterization using a single-shot version of frequency-resolved optical gating (FROG) called GRENIOULLE.[27] Using a Fresnel biprism, a single pulse is split into two pulses that cross at variable delays inside a nonlinear crystal depending on their position in space. The second harmonic light is then frequency resolved by phase matching within the crystal and measured with a two-dimensional CCD camera. Recently, the same principle was used to record a single-shot transient grating FROG (TG FROG),[23] which is not limited by the bandwidth limitations of the nonlinear doubling crystal. Of these methods, the GRAPE spectrometer is most conceptually similar to the single-shot TG design. GRAPE, however, uses an additional heterodyne pulse and Fourier transformation along the spatially encoded delay dimension.

Recently, another single-shot method using angular rather than spatial encoding was introduced by Mercer et al.[28] to resolve the transition energies involved in a particular Feynman pathway. This angle-resolved coherent (ARC) optical wave-mixing method takes advantage of the frequency-dependent phase matching geometry to separate coherently coupled quantum transitions from energy transfer. Another elegant single-shot approach was demonstrated by DeCamp et al. to capture a two-dimensional spectrum in the frequency domain.[29] Both these methods differ from two-dimensional photon echo spectroscopy in several ways. For example, the ARC method separates response pathways

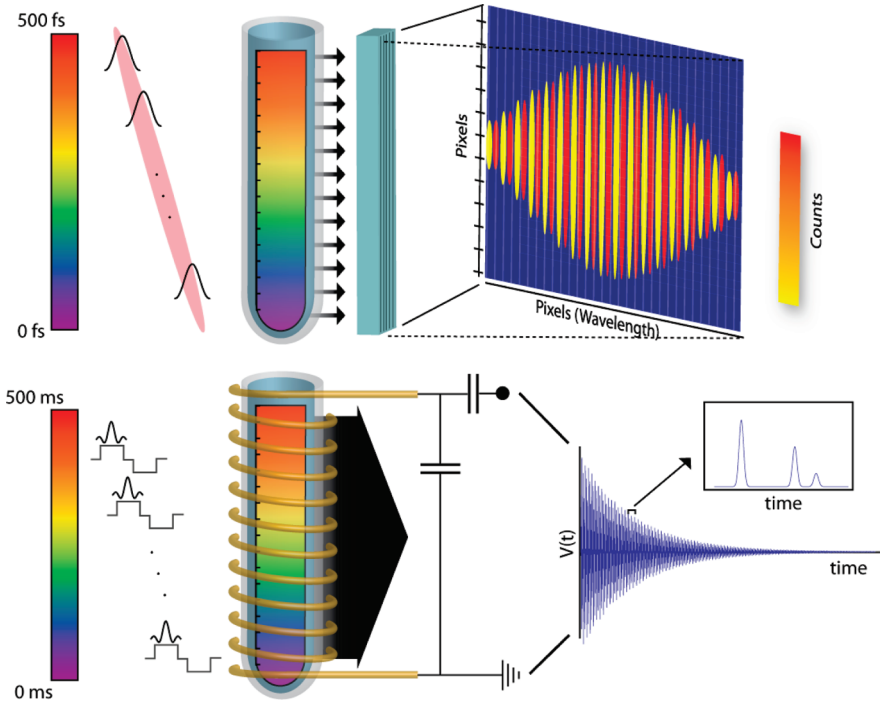

Figure 4. Analogy to MRI. Similarities and differences of single scan NMR and GRAPE methods. A heterogeneous excitation of the sample is achieved via the use of tilted wavefront with GRAPE and a magnetic field gradient with chirped-pulse excitation in single scan NMR. The signal in GRAPE is spectrally resolved onto a two-dimensional CCD via the use of a grating and interfered with a reference to yield the magnitude and phase of the resulting signal. In single-scan NMR, an echo planar chemical-shift imaging protocol is used to encode the chemical information into the free induction decay, which is monitored by the use of a coil around the sample.

while sacrificing time resolution and separation of inhomogeneous from homogeneous broadening.

CONNECTION TO MRI

Our motivation to develop GRAPE spectroscopy arises from attempting to exploit the connection between NMR and nonlinear optical spectroscopy by extending the analogy to magnetic resonance imaging (MRI). MRI is well-known as an unparalleled imaging tool used to peer inside the human body. However, it was not until decades after its inception that the method came into widespread use. The discovery by Mansfield and co-workers that rapid gradient switching could produce images in a single transient[30] propelled the technique, known as echo planar imaging (EPI), from the laboratory to the clinical setting. EPI capitalizes on the reversible nature of the Zeeman interaction to acquire multiple spin echoes within a single time course. The cousin of MRI, nuclear magnetic resonance (NMR) spectroscopy, is conceptually similar.[17] Yet, MRI, which can be viewed as a multidimensional correlation technique that correlates spins in space across orthogonal spatial dimensions, and multidimensional NMR spectroscopy, which correlates frequencies over several spectral dimensions, differ significantly in their sampling schemes.[31,7] Fundamentally, due to the irreversibility of the chemical shift and indirect couplings that serve to define the features in the NMR spectrum, multidimensional NMR spectroscopy requires a slow, multiscan acquisition scheme in which the indirect temporal dimension is systematically scanned prior to Fourier transformation, regardless of the available sensitivity.

Recently, a powerful single-scan method in NMR introduced by Frydman et al. was shown to circumvent this limitation by recording the entire multidimensional NMR spectrum in a single-scan utilizing imaging gradients on a homogeneous sample.[32,33] Whereas the goal of imaging is to resolve spatial inhomogeneity, utilizing imaging gradients on a homogeneous sample allows for a parallel encoding of the indirect time domain in space. In its simplest incarnation, a radio frequency sweep is applied to the sample in the presence of a pulsed gradient to uniformly excite each position in the sample at a different moment in time. Owing to the linearity of the sweep and gradient, spins along the gradient axis undergo a phase evolution directly proportional to their position along the gradient. After a mixing sequence and a single Fourier transformation along the direct time domain, a suitable unwrapping of this spatial encoding results in an *n*-dimensional NMR spectrum.

While the analogy between optical spectroscopy and NMR has been appreciated for many years,[34] the connection to MRI has thus far been neglected, even though NMR and MRI have been successfully merged with the advent of molecular imaging[35] and single-scan spectroscopy. As shown in Figure 4, GRAPE spectroscopy and single-scan NMR share many similarities, although each uses very different types of gradients: NMR utilizes magnetic field gradients, while the gradient in GRAPE is imposed purely geometrically. Unlike the NMR case, GRAPE achieves no loss in signal even though the acquisition time is reduced by several orders of magnitude by eliminating an entire experimental dimension. This difference is fundamentally tied to the ratio of the wavelength to the sample size. In NMR, the wavelength is long compared to the sample, and the signal is emitted from the entire sample. In the optical regime, the wavelength is short compared to the sample, permitting tight focusing such that only a small portion of the sample emits signal.

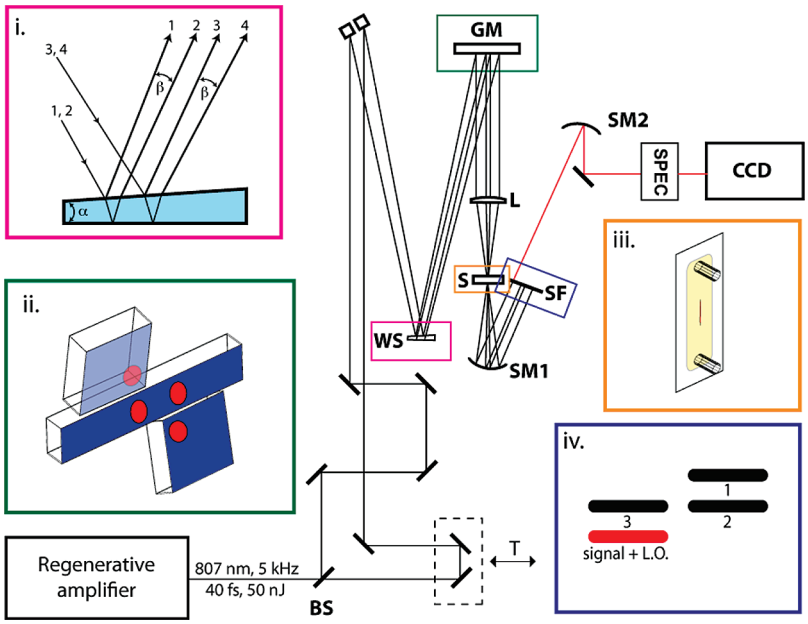

Figure 5. Optical setup of single-shot GRAPE spectroscopy. Two beams resulting from passing a 40 fs, 50 nJ pulse through a beam splitter (BS) are delayed by a time, *T*, with respect to one another by a motorized translation stage. These time-delayed beams pass through a wedged beam splitter (WS, inset i) to form the four beams, $\mathbf{k}_1-\mathbf{k}_4$, used in the GRAPE pulse sequence. These beams, arranged in a distorted boxcar geometry, then reflect off the GRAPE mirror assembly (GM, inset ii) toward a cylindrical lens (L) which focuses the beams along the *x*-axis of the sample (S, inset iii). The emitted nonlinear signal is imaged onto the entrance slit of a spectrometer (SPEC) by two spherical mirrors (SM1 and SM2) that form a 2× telescope. The signal and local oscillator are isolated from the pump beams using a spatial filter (SF, inset iv) before detection by a thermoelectrically cooled CCD camera.

By focusing on a larger area (a line) within the sample, we can acquire more information without sacrificing signal.

EXPERIMENTAL APPARATUS

A schematic of the optical layout is shown in Figure 5. A Ti:sapphire oscillator (Micra, Coherent Inc.) is used to seed a regenerative amplifier (Legend Elite USP-HE, Coherent Inc.) to generate 40 fs pulses centered at 807 nm at a 5 kHz repetition rate. The pulse length is measured using single-shot second harmonic frequency-resolved optical gating (Grenouille, Swamp Optics) prior to the sample. A small fraction of the amplifier output pulse (20 μJ) passes through a beam splitter, creating two beams, each with a 1/e diameter of roughly 6 mm. The relative delay between the beams is controlled by a motorized translation stage (Aerotech Inc.), which defines the population time, *T*. The beams are then further split into two pulse pairs, creating four pulses, labeled here as $\mathbf{k}_1-\mathbf{k}_4$, by the use of front and back Fresnel reflections from a 3 mm thick uncoated 3° wedged optic (Figure 5i). The wedged optic provides a convenient means of dumping excess pulse energy and reduces the number of optical components by eliminating additional pairs of beam splitters and mirrors necessary to steer the beams back toward the sample. The incident angles of the two horizontally and vertically displaced input beams to the wedged optic are adjusted such that the Fresnel reflection of the rear surface of one wedge ($\mathbf{k}_2$) is parallel to the Fresnel reflection from the front surface of the other ($\mathbf{k}_3$). The remaining two reflections form beams $\mathbf{k}_1$ and $\mathbf{k}_4$. To compensate for dispersive effects within the wedge, compensating 6 mm fused silca plates are inserted into the two beams emanating from Fresnel reflections from the front surfaces. The four beams are aligned to form the distorted boxcar geometry shown in Figure 3B.

To generate the requisite temporal gradients at the sample, the four beams are reflected off a mirror assembly, which we refer to as the GRAPE mirror, as shown in Figure 5ii. Beams 2 and 3 reflect off a single mirror while pulses 1 and 4 reflect off separate mirrors, each mounted on a delay stage that acts to compensate for temporal delays caused by the finite thickness of the wedged beamsplitter. The beam 4 mirror is mounted on an independent translation stage to control the timing of beam 4 with respect to the other beams. To avoid pump−probe effects, beam 4 is adjusted such that it arrives before beams 1, 2, and 3. All four beams then pass through a cylindrical lens with a 250 mm focal length, which focuses the beams in the horizontal dimension to a 40 μm wide, 6 mm tall focal line at the sample (Figure 5iii). In the vertical direction, beams 1 and 4 are directed toward the sample where they overlap with beams 2 and 3. The vertical angle, α, at which beam 1 crosses beam 2, serves to define the temporal gradient. This gradient can be adjusted by changing the distance of the cylindrical lens and sample from the GRAPE mirror or, alternatively, by adjusting the distance from the wedged optic to the GRAPE mirror while maintaining the distance between the GRAPE mirror and the sample. The vertical angle in which beam $\mathbf{k}_4$ is directed toward the sample is roughly negative in sign to the vertical angle in which $\mathbf{k}_1$ is directed toward the sample. These two angles serve to define the timing of the signal relative to the echo and hence the slope of the echo signals relative to the τ axis.

For heterodyne detection, beam four is attenuated by utilizing the front Fresnel reflection from an optical flat and a neutral density filter placed after the mirror assembly, resulting in a total attenuation of roughly 3 orders of magnitude. At the sample, the energy of pulses $\mathbf{k}_1-\mathbf{k}_3$ is roughly 50 nJ per pulse, which results in an energetic flux of 20 μJ/cm^2, comparable to point-by-point methods. The sample, 0.4 mM IR144 in methanol, is recirculated through a flow cell (Starna) by a peristaltic pump (Cole Parmer).

dx.doi.org/10.1021/jp107022f |*J. Phys. Chem. A* 2011, 115, 3787–3796

Two spherical optics of focal lengths 50 and 25 cm image the emitted signal (effectively a line source) from the μm slit at the spectrometer (Andor). To isolate only the signal and local oscillator, a spatial filter is placed roughly 25 cm after the first spherical mirror. At this location, all four beams separate in the horizontal direction, allowing beams $\mathbf{k}_1-\mathbf{k}_3$ to be blocked for background-free detection (Figure 5iv). After passage through the spatial filter, the heterodyned signal is spectrally resolved using a 1200 lines/mm diffraction grating and a 2048 × 2048 thermoelectrically cooled CCD array (Andor). The resulting interference pattern enables determination of the phase and magnitude of the signal. 2D spectra were recorded for various population times from T = 0 to T = 100 fs in steps of 10 fs. All measurements were taken at ambient temperature, 21 °C.

RESULTS AND DISCUSSION

Pulse Timings. The spatially encoded pulse timings that in aggregate make up the whole Fourier sampling for GRAPE are determined by spectral interferometry.[36] The relative timings between pulse pairs is derived by measuring the scatter of beams 1 and 3 from a microscope slide at the position of the sample in the direction of beam 4. Due to uncertainty in the interferometric measurement in the presence of noise, we found that aligning beams 2 and 3 optically ensured the smallest gradient in population time. The alignment was done by projecting beams 2 and 3 several meters and adjusting the input angle of one of the beams such that the two beams were parallel to better than 10^{-4} radians. For beams 1 and 3, the interference between the scattered light and beam 4 at the sample position is imaged onto the spectrometer slit and then spectrally resolved by a diffraction grating prior to detection by the CCD. Owing to the imaging aspect of the GRAPE spectrometer, it is possible to measure simultaneously several scattering events along the spatially encoded axis. This approach allows the slopes of the temporal delays of each beam, 1 and 3, relative to beam 4 to be measured in a single shot (Figure 6, left). Due to the nonuniformity of the scattering medium, in practice only a few positions along y are useful for accurate spectral interferometric analysis. Knowledge of the pulse timings, t_{i4} with i = 1, 2, or 3, relative to a single pulse (i.e., beam 4) then uniquely determines the entire spatially encoded pulse sequence (Figure 6, right). The crossing point between lines t_{14} and t_{24} serves to define the detector pixel along y that corresponds to τ = 0. From these timings, we obtain $\partial\tau/\partial N$ = 0.57 ± 0.05 fs/pixel and $\partial T/\partial N$ < 0.01 fs/pixel, where N is pixels. This value of $\partial\tau/\partial N$ allows frequencies as high as 11.0 rad/fs (170 nm) to be detected, well above the optical frequencies of visible light. A low value of $\partial T/\partial N$ ensures that the population time across the sample remains constant. In this experiment, the population time is constant to less than 4 fs across the sample, sufficient to resolve population dynamics of IR144 in methanol. Because the focus at the sample is imaged onto the spectrometer slit by a 2× telescope and each camera pixel is 13.5 μm in height, we measure to $\partial\tau/\partial z$ = 84.0 ± 8 fs/mm and $\partial T/\partial z$ < 1 fs/mm at the sample. By adjustment of the beam 1 delay, the crossing point can be positioned anywhere across the unfocused beam waist. The crossing point was chosen such that the majority of the signal resulted from positive τ values (beam 1 before beam 2), which correspond to rephasing signal pathways. The range of τ values selected to lie within the full-width at half-maximum (fwhm) of the beam waist along the spatially encoded direction is approximately −50 fs < τ < 230 fs. Negative τ values ensure that pulse overlap is taken into account. Purely nonrephasing signal was not collected because negative τ values also involve mixed T values in the $\mathbf{k}_s = -\mathbf{k}_1 + \mathbf{k}_2 + \mathbf{k}_3$ direction.

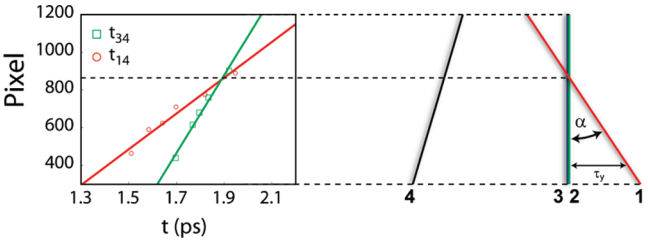

Figure 6. Pulse timings. Spatially encoded pulse timings are determined by analyzing the interferogram resulting from scatter between beams 1 and 3 with beam 4 at the position of the sample. Scatter points with high fringe contrast are selected for analysis by spectral interferometry to give $t_{34}(y)$ (green boxes) and $t_{14}(y)$ (red circles). Linear regression plots determine the temporal gradients of beams 1 and 3 relative to beam 4 (green and red solid lines, respectively): $dt_{1,4}/dy$ = 1.05 ± 0.1 fs/pixel and $dt_{3,4}/dy$ = 0.48 ± 0.05 fs/pixel. The crossing point, y_i, at which $\Delta t_{14}(y_i) = \Delta t_{34}(y_i)$ defines τ = 0 assuming that $\Delta t_{34}(y) = \Delta t_{24}(y)$ at T = 0. These timings serve to define the spatially encoded pulse sequence shown schematically to the right.

Photon Echo Signal. The raw signal in the phase-matched direction $\mathbf{k}_s = -\mathbf{k}_1 + \mathbf{k}_2 + \mathbf{k}_3$ is heterodyned with a reference beam, $\mathbf{k}_4$, and imaged onto a CCD detector. To eliminate unwanted scatter contributions, we employ a sequence of shutter configurations to record the scatter of beams 1, 2, and 3 in the direction of the signal. The scatter-subtracted heterodyne signal at T = 0 as shown in Figure 7A is given by $I_S = I_{1234} - I_{124} - I_{34} + I_4$, where the subscript indicates which beams were unblocked during the signal acquisition.[9] The vertical stripes result from the interference between the third-order signal and the heterodyne pulse along each position in the sample. A horizontal cut through the heterodyned signal reveals the interference signal as shown in Figure 7B. The time delay between the local oscillator (LO) and the photon echo signal determines the frequency of this signal. From the pulse timing data in Figure 6, each pixel along the vertical axis maps to a unique τ value according to $\tau = N \times (\partial\tau/\partial N)$. To isolate only the photon echo signal that forms approximately $\tau(y)$ after pulse 3, the heterodyned signal must first be transformed into the τ/t domain. Because the signal is naturally recorded across a wavelength rather than frequency axis, we convert the linear wavelength axis to a linear frequency axis using Fourier interpolation as described previously.[36] Following Fourier transformation along the t domain and appropriate windowing to remove the homodyne contribution to the signal, a photon echo as a function of τ is formed as shown in Figure 7C. The integrated echo peaks at about τ = 20 fs as expected from previous photon echo peak shift studies on IR144.[6] Due to pulse overlap effects, signal at negative τ values is expected. For τ values larger than the pulse duration, coherent oscillations between the ground and excited state of the molecule lead to formation of a photon echo signal that persists to about τ = 100 fs—again in agreement with previous studies of IR144 in methanol at room temperature. Fourier transformation of the echo signal with respect to τ shows a peak centered near zero frequency as expected for rotating frame detection (Figure 7D). A small deviation from zero results from a dynamic Stokes shift within the pulse temporal envelope at T = 0.

Pump-Probe. Unlike NMR, the relative phase of pulses comprising the 2D pulse sequence is generally unknown.

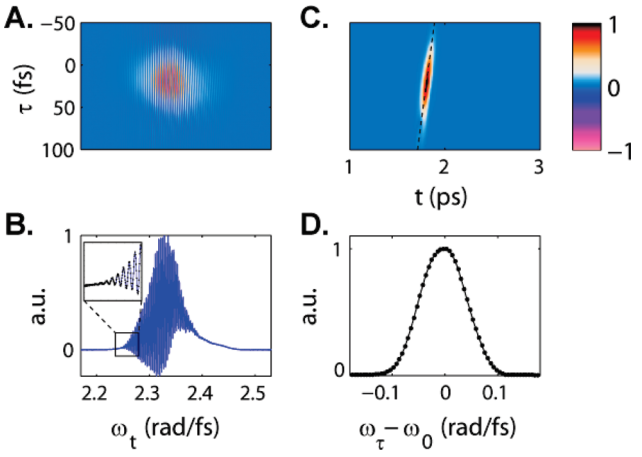

Figure 7. (A) Scatter-subtracted raw signal. Background subtracted heterodyned signal after Fourier interpolation (see text) is given by $I_S = I_{1234} - I_{124} - I_{34} + I_4$. The vertical pixel axis is converted to τ values according to measurements taken by spectral interferometry (see Figure 6). (B) Projection of the raw signal along τ. An interferogram is formed by interference of the signal with the local oscillator. Oscillation frequency is given by the timing between pulse 4 and the signal. The inset shows an enlarged area of the heterodyned signal showing high fringe contrast and high signal-to-noise. (C) Photon echo signal. Fourier transformation of the Fourier interpolated signal in (A) about ω_t results in a $\tau-t$ plot containing the homodyne and photon echo signals. After windowing to remove the homodyne signal, an echo appears at roughly 1.8 ps after pulse 4. (D) Rotating frame detection. Fourier transformation of a cut through the photon echo signal (dashed line in (C)) about τ confirms that the signal in GRAPE is measured in the rotating frame. The line width of the signal is given by a convolution of the linear absorption spectrum and the laser spectrum.

Knowledge of the absolute phase of the spectrum is necessary to separate dispersive and absorptive components of the line shape. Since electronic spectra are generally very broad, eliminating dispersive line shape contributions is critical for optimizing spectral resolution, even in photon echo spectroscopy where the homogeneous line width along the antidiagonal direction is recovered. In NMR, this "phasing" procedure is routinely accomplished by multiplying the spectrum by a zero-order and first-order phase term until negative features disappear, indicating purely absorptive line shapes. In the optical regime, phasing by eye is generally more difficult because of four-level contributions of dipole products, which may give negative features even in the purely absorptive spectra. Also, the existence of excited state absorption in some systems leads to a decrease in signal, which manifests itself as a negative feature in the 2D spectrum. To phase 2D optical spectra, the projection-slice theorem is used. This theorem states that the Fourier transform of a slice through the center of a function, f, is equal to the projection of the two-dimensional Fourier transform of f along a line parallel to that slice. If we consider our function to be $f(\tau,t)$, then the projection-slice theorem states that

$$F_{t,\tau}P_{\omega_\tau}f(\tau,t) = S_{\tau=0}F_t f(\tau,t) \quad (1)$$

where F, P, and S are Fourier transform, projection, and slice operators, respectively. The term on the left is equal to the projection of the real part of the two-dimensional spectrum, $f(\omega_\tau,\omega_t)$, while the term on the right is equivalent to spectrally resolved pump-probe signal. Therefore, a separate measurement

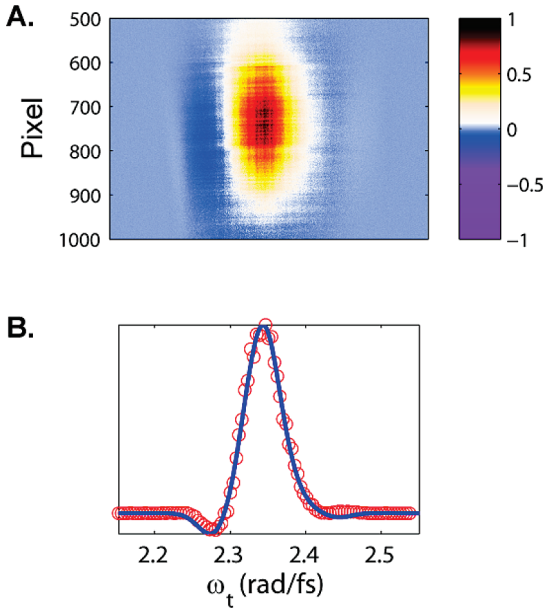

Figure 8. (A) $T = 0$ spectrally resolved pump−probe signal. Beams 2 and 3 are used as the pump and probe pulses, respectively. Since the wavefronts of beams 2 and 3 are parallel at the focus of the cylindrical lens, the entire illuminated region of the sample contributes to the pump-probe signal. (B) Phasing of 2D spectra. The projection of the real part of the 2D spectrum (blue solid curve) is "phased" to match the projection of the pump−probe image in (A) along the vertical axis of the detector (red circles).

of the pump−probe signal provides an independent means of determining the absolute phase of the 2D spectrum.

Unfortunately, spectrally resolved pump−probe data are difficult to acquire with CCD cameras because of the large probe background signal relative to the very small pump−probe signal. Typically, one resorts to using a lock-in amplifier and monochromator to record weak pump−probe signals at each desired wavelength. However, such long integration times and slow point-by-point acquisitions makes this approach undesirable. Furthermore, it would largely negate the benefits of single-shot spectroscopy for anything but the absolute value 2D spectra. Here, we have managed to circumvent the very poor signal-to-noise of spectrally resolved pump−probe by employing a variation of the GRAPE method. To measure the pump−probe signal, we utilize beam 2 as the pump and beam 3 as the probe. Since the wavefronts of these two beams are parallel to one another at the sample, we can record a pump−probe signal across the entire unfocused beam diameter rather than at a single focused point. The signal-to-noise ratio (SNR) then increases by a factor of roughly $(R_y/R_x)^{1/2}$ where R_x and R_y are the beam diameters at the sample in the focused and unfocused directions, respectively. For our particular apparatus this approach yields a factor of 10 improvement in SNR or a factor of 100 in reduced signal averaging over a point-by-point approach. As shown in Figure 8, each pixel on the camera along the axis of the sample contributes to the pump−probe signal. The uniformity of the signal for IR144 at $T = 0$, which has very fast dynamics relative to the pulse duration, confirms the absence of a significant 2/3 temporal gradient. Averaging the pump−probe signal over the vertical axis of the CCD area results in sufficient SNR for phasing even without signal averaging. Therefore, pump−probe measurements take about half the time to acquire as the 2D spectrum,

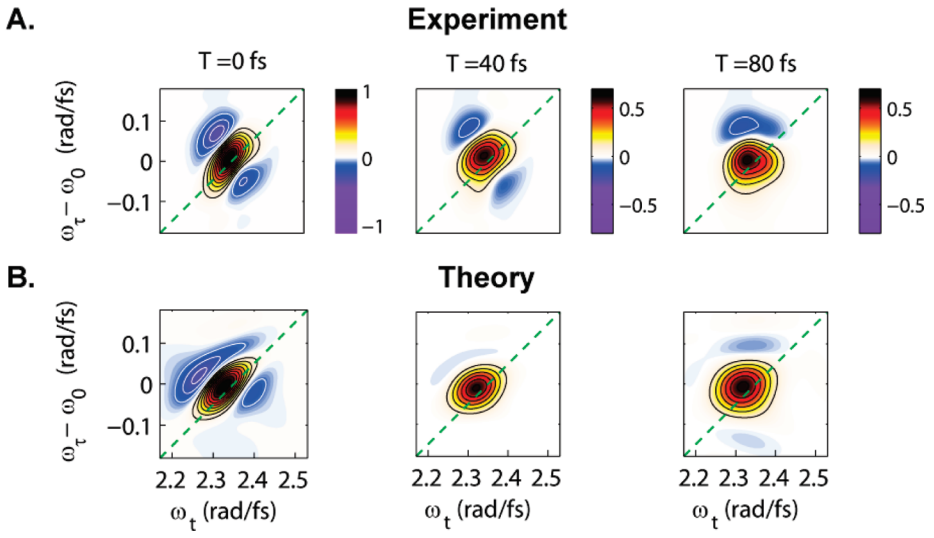

Figure 9. (A) Experimental rephasing 2D spectra. Real part of rephasing 2D spectra of 0.4 mM IR144 in methanol at $T = 0$, 40, and 80 fs. Contour lines are drawn at 10% increments of the $T = 0$ real maximum. The negative amplitude is represented by dotted contours. The vertical dimension is given by $\omega_\tau - \omega_0$ because the coherence frequency is detected in the rotating frame. Deviation of the central peak from the diagonal (dotted line) results from a dynamic Stokes shifted emission. (B) Theoretical rephasing 2D spectra. Calculated real part of the rephasing 2D spectra of IR144 in methanol at $T = 0$, 40, and 80 fs are shown. Contour lines are drawn at 10% increments of the $T = 0$ real maximum. Negative amplitude is represented by dotted contours. The calculation used 40 fs transform-limited pulses centered at 807 nm.

which requires four individual frame transfers for each population time. Phasing the 2D spectrum then proceeds by multiplying the projection of the real part of the 2D spectrum by a phase factor,

$$\Phi_0 + (\omega_t - \omega_0)\partial\Phi_0/\partial\omega + (\omega_t - \omega_0)^2\partial^2\Phi_0/\partial\omega^2 \qquad (2)$$

to match the pump−probe signal. The zero-order term corresponds to an overall phase constant correction, while the linear term corrects for uncertainties in the $t_{34}(y)$ timing. A small quadratic term is applied to correct for minor dispersive terms owing to pulse chirp and dispersion in the system. The real part of the 2D spectra and separately recorded pump−probe spectra are in excellent agreement at all population times measured after this phasing procedure. While technically the projection-slice theorem is only applicable to the total 2D spectrum rather than the rephasing part alone, the nonrephasing contribution to the signal in IR144 is negligible and therefore this approximation does not affect our result.

Unlike point-by-point methods, an additional phasing parameter must be taken into account owing to the way in which the τ domain is sampled. Errors in determination of $\tau = 0$ from spectral interferometry as described earlier result in additional phase roll in the ω_τ dimension. Fitting the projection of the 2D spectrum along ω_τ to the linear absorption spectrum makes phasing along that axis possible. If excited state absorption is neglected, this approach is just another application of the projection slice theorem about a perpendicular slice at $t = 0$. Although not strictly true because the absorption spectrum is a linear, rather than a third-order process, this approach provides a reliable, practical means of phasing along τ. The phase correction takes the form

$$\Phi_0'(\omega_t - \omega_0)\tau_c \qquad (3)$$

where τ_c corrects for the timing error in the determination of $\tau = 0$.

2D Spectra of IR144. Once the absolute phase of the spectrum is determined, the real part of the rephasing spectrum is generated as shown in Figure 9A. In agreement with previous reports on IR144, a small negative feature above the main diagonal is observed in the real part of the 2D spectrum at $T = 0$. This feature can be attributed to four-level contributions that involve vibrationally excited states on the ground electronic surface. At room temperature, cross peaks are poorly resolved due to fast relaxation relative to the pulse duration resulting from strong coupling of the vibronic levels to the solvent. Because GRAPE is a photon echo spectroscopy, a narrower line width in the antidiagonal direction is observed compared to the homogeneous line width at $T = 0$. At $T = 40$ fs, the system begins to lose memory and the diagonal peak becomes rounder. That is, transition energies during the initial excitation period quickly lose correlation as the bath motions induce spectral diffusion. By $T = 80$ fs, transition energy correlation between absorption and emission completely disappears and the slope of the center peak nears zero. In Figure 9B, simulations of the rephasing part of the 2D photon echo spectra are shown. The details of the numerical calculations of the third-order polarization are given elsewhere.[3,9] Briefly, we model the chromophore as consisting of two electronic states. The transition energy correlation function is then modeled by considering contributions from the solvent as a collection of harmonic oscillators linearly coupled to the chromophore (i.e., a multimode Brownian oscillator model). The solvent contribution contains a fast inertial contribution, which we model as Gaussian, and two diffusive modes modeled as exponentials. The simulated spectra reproduce all the major features of the experimental data. A small negative feature is observed below the diagonal in both the experimental and simulated data at $T = 0$. This feature has not been previously observed in experimental spectra of IR144 in methanol. Also, not previously observed experimentally, but reproduced in the simulations, are small negative features above the main diagonal for population times greater than $T = 20$ fs. We believe our ability to resolve these features stems from the significantly higher SNR offered by GRAPE, primarily in the reduction of so-called

multiplicative noise, compared to point-by-point acquisition protocols. In multiscan 2D spectroscopy, parametric sampling of τ is susceptible to multiplicative or t_1 noise in the NMR jargon, so named because it primarily affects the indirect dimension (i.e., τ dimension in 2D ES or t_1 dimension in 2D NMR) of 2D spectroscopic experiments. Primarily in the form of phase errors, t_1 noise may be transferred to the emitted signal as a result of sample fluctuations, ultimately leading to line broadening and reduced signal-to-noise (SNR) in the spectrum. GRAPE eliminates problems that arise from nonuniform temporal sampling or fluctuations in laser power, temperature, alignment, index of refraction, or laser spectrum. A quantitative analysis of t_1 noise in GRAPE versus multiscan acquisition schemes will be the subject of a future publication.

Other Considerations. For the proof-of-principle experiment presented here, only the rephasing contribution to the 2D spectra is recorded. Simulated 2D spectra of IR144 show that the nonrephasing signal is negligible for negative delays beyond the pulse overlap regime. However, for other systems recording the nonrephasing contribution may be necessary for obtaining purely absorptive lineshapes, rather than phase-twisted line shapes that result from an unbalanced combination of coherence pathways. Unlike point-by-point acquisition, it is not possible, in general, to utilize the spatial region where $\tau < 0$ because this region contains mixed population times in the phase-matched direction, $\mathbf{k}_s^{rp} = -\mathbf{k}_1 + \mathbf{k}_2 + \mathbf{k}_3$. However, it is possible to observe directly the nonrephasing signal, $\mathbf{k}_s^{nrp} = \mathbf{k}_1 - \mathbf{k}_2 + \mathbf{k}_3$. Heterodyning this signal requires an additional local oscillator, but because of the single-shot nature of GRAPE, phase stabilization is no longer required. In fact, the wedged optic already provides a beam in the position of the phase-matched geometry corresponding to the nonrephasing signal. Therefore, incorporating an additional pulse is relatively straightforward. Furthermore, since only a small area of the CCD sensor is used for rephasing signal detection, another area of the sensor could, in principle, be used to record the nonrephasing signal simultaneously. This approach would provide an additional savings of a factor of 2 in signal acquisition time. Future implementations of GRAPE will incorporate this capability.

Another potential artifact arises from the nonuniform spatial profile across the unfocused beam waist. Since the signal is proportional to the third power of the electric field, the beam profile will act to weight τ points differently. However, in principle this effect can be corrected for in the postprocessing provided sufficient SNR. Furthermore, it should be possible to create flattop beam profiles, which would eliminate this effect entirely or even to exploit it as an apodization mechanism for enhanced resolution. Finally, the spectrometer used to record these spectra was designed for spectroscopic rather than imaging applications. Therefore, the echo signal emitted from the sample in the form of a line and imaged onto the spectrometer entrance slit does not properly focus onto the imaging plane of the CCD camera. Curvature-of-field effects further distort the echo shape and ultimately give rise to spectral, broadening in the 2D spectra although this broadening can be removed in the postprocessing. At low optical density, we expect GRAPE to outperform traditional methods as a higher sensitivity is expected.

Pulse Power. While GRAPE spectroscopy achieves a reduction in acquisition time by spreading the beam across the sample, it does so at the cost of increased pulse energy to maintain an equivalent flux. For example, for a 6 mm beam waist, the additional pulse energy required is a factor of 100 compared to a beam focused to 60 μm. However, since most 2D experiments operate in the weak-field limit, the additional pulse power is easily achievable. In this experiment, the output power of the regenerative amplifier was attenuated by more than 10^4. Therefore, even outside the fundamental laser frequency of the amplifier output, ample power exists to run GRAPE at other wavelengths after passage through an OPA, which typically achieves efficiency above 10%.

We note that while the minimum exposure time of our CCD camera prevented acquisition of the 2D spectrum in a single laser-shot, GRAPE can achieve high SNR even in a single laser shot. For IR144 at $T = 0$, the SNR exceeds 5000 at the 5 kHz repetition rate of the laser, indicating that a single laser pulse generates an SNR exceeding 70.

CONCLUSION

We demonstrate a single-shot method to obtain two-dimensional electronic spectra in real-time. The acquisition time of 2D ES has decreased from several minutes to a fraction of a second without loss in signal. In addition, GRAPE achieves an increase in signal-to-noise in the 2D spectrum of IR144, allowing us to observe features previously undetected by point-by-point methods. The inherent phase stability of the GRAPE method eliminates the need for passive and active phase stabilization. Combined with a significantly simplified optical setup, GRAPE has the potential to bring 2D optical spectroscopy into more widespread use due to relaxed experimental constraints. The orders of magnitude reduction in acquisition time will permit practical implementation of higher-order optical spectroscopy to resolve congested spectral features as well as real-time monitoring of irreversible chemical dynamics, adaptive materials, and photodamage with fast imaging detectors.

ACKNOWLEDGMENT

We thank the NSF MRSEC (DMR 08-00254), AFOSR (FA9550-09-1-0117), and the Searle Foundation for Support. E.H. acknowledges support from the National Science Foundation Grant DMR-0844115 and the Institute for Complex Adaptive Matter Branches Cost-Sharing Fund. A.F.F. acknowledges support from the DOE SCGF program.

REFERENCES

(1) Jimenez, R.; Fleming, G. R.; Kumar, P. V.; Maroncelli, M. *Nature* **1994**, *369*, 471.
(2) Maroncelli, M.; Macinnis, J.; Fleming, G. R. *Science* **1989**, *243*, 1674.
(3) Mukamel, S. *Principles of Nonlinear Optical Spectroscopy*; Oxford University Press: New York, NY, U.S., 1995.
(4) Brixner, T.; Stenger, J.; Vaswani, H. M.; Cho, M.; Blankenship, R. E.; Fleming, G. R. *Nature* **2005**, *434*, 625.
(5) Cowan, M. L.; Ogilvie, J. P.; Miller, R. J. D. *Chem. Phys. Lett.* **2004**, *386*, 184.
(6) Hybl, J. D.; Ferro, A. A.; Jonas, D. M. *J. Chem. Phys.* **2001**, *115*, 6606.
(7) Aue, W. P.; Bartholdi, E.; Ernst, R. R. *J. Chem. Phys.* **1976**, *64*, 2229.
(8) Brixner, T.; Stiopkin, I. V.; Fleming, G. R. *Opt. Lett.* **2004**, *29*, 884.
(9) Brixner, T.; Mancal, T.; Stiopkin, I. V.; Fleming, G. R. *J. Chem. Phys.* **2004**, *121*, 4221.
(10) Cho, M. H. *Chem. Rev.* **2008**, *108*, 1331.
(11) Jonas, D. M. *Annu. Rev. Phys. Chem.* **2003**, *54*, 425.

(12) Cho, M. H.; Fleming, G. R. *J. Chem. Phys.* **2005**, *123*, .
(13) Stone, K. W.; Gundogdu, K.; Turner, D. B.; Li, X. Q.; Cundiff, S. T.; Nelson, K. A. *Science* **2009**, *324*, 1169.
(14) Milota, F.; Sperling, J.; Nemeth, A.; Abramavicius, D.; Mukamel, S.; Kauffmann, H. F. *J. Chem. Phys.* **2009**, *131*, .
(15) Nemeth, A.; Milota, F.; Sperling, J.; Abramavicius, D.; Mukamel, S.; Kauffmann, H. F. *Chem. Phys. Lett.* **2009**, *469*, 130.
(16) Engel, G. S.; Calhoun, T. R.; Read, E. L.; Ahn, T. K.; Mancal, T.; Cheng, Y. C.; Blankenship, R. E.; Fleming, G. R. *Nature* **2007**, *446*, 782.
(17) Ernst, R. R.; Bodenhausen, G.; Wokaun, A. *Principles of nuclear magnetic resonance in one and two dimensions*; Oxford University Press: Oxford, U.K., 1987.
(18) Jonas, D. M. *Science* **2003**, *300*, 1515.
(19) Vaughan, J. C.; Hornung, T.; Feurer, T.; Nelson, K. A. *Opt. Lett.* **2005**, *30*, 323.
(20) Tian, P. F.; Keusters, D.; Suzaki, Y.; Warren, W. S. *Science* **2003**, *300*, 1553.
(21) Volkov, V.; Schanz, R.; Hamm, P. *Opt. Lett.* **2005**, *30*, 2010.
(22) Yetzbacher, M. K.; Belabas, N.; Kitney, K. A.; Jonas, D. M. *J. Chem. Phys.* **2007**, *126*, .
(23) Nagy, T.; Simon, P. *Opt. Express* **2009**, *17*, 8144.
(24) Topp, M. R.; Rentzepis, P. M.; Jones, R. P. *Chem. Phys. Lett.* **1971**, *9*, 1.
(25) Poulin, P. R.; Nelson, K. A. *Science* **2006**, *313*, 1756.
(26) Fourkas, J. T.; Dhar, L.; Nelson, K. A.; Trebino, R. *J. Opt. Soc. Am. B* **1995**, *12*, 155.
(27) Kane, D. J.; Trebino, R. *Opt. Lett.* **1993**, *18*, 823.
(28) Mercer, I. P.; El-Taha, Y. C.; Kajumba, N.; Marangos, J. P.; Tisch, J. W. G.; Gabrielsen, M.; Cogdell, R. J.; Springate, E.; Turcu, E. *Phys. Rev. Lett.* **2009**, *102*, .
(29) DeCamp, M. F.; DeFlores, L. P.; Jones, K. C.; Tokmakoff, A. *Opt. Express* **2007**, *15*, 233.
(30) Stehling, M. K.; Turner, R.; Mansfield, P. *Science* **1991**, *254*, 43.
(31) Edelman, R. R.; Hesselink, J. R.; Zlatkin, M. B. *Clinical magnetic resonance imaging*, 3rd ed.; Saunders Elsevier: Philadelphia, PA, U.S., 2006.
(32) Frydman, L.; Scherf, T.; Lupulescu, A. *Proc. Natl. Acad. Sci. U. S. A.* **2002**, *99*, 15858.
(33) Mishkovsky, M.; Frydman, L. *Annu. Rev. Phys. Chem.* **2009**, *60*, 429.
(34) Hahn, E. L. *Concepts Magn. Reson.* **1997**, *9*, 69.
(35) Sosnovik, D. E.; Weissleder, R. *Curr. Opin. Biotechnol.* **2007**, *18*, 4.
(36) Dorrer, C.; Belabas, N.; Likforman, J. P.; Joffre, M. *J. Opt. Soc. Am. B* **2000**, *17*, 1795.